



Sn_{0.9}In_{0.1}P₂O₇-Based Organic/Inorganic Composite Membranes Application to Intermediate-Temperature Fuel Cells

Pilwon Heo,^{a,*} Masahiro Nagao,^{a,*} Toshio Kamiya,^a Mitsuru Sano,^a
Atsuko Tomita,^b and Takashi Hibino^{a,*,z}

^aGraduate School of Environmental Studies, Nagoya University, Nagoya 464-8601, Japan

^bNational Institute of Advanced Industrial Science and Technology, Nagoya 463-8560, Japan

An anhydrous proton conductor, 10 mol % In³⁺-doped SnP₂O₇ (Sn_{0.9}In_{0.1}P₂O₇), was composed by 1,8-bis(triethoxysilyl)octane (TES-Oct) and 3-(triethoxysilyl)-1-propanesulfonic acid ((THS)Pro-SO₃H) and was characterized by structural and electrochemical analysis. The composite membrane with 90 wt % Sn_{0.9}In_{0.1}P₂O₇ showed high proton conductivities of 0.04 S cm⁻¹ or more between 150 and 200 °C in unhumidified air. The packing of the Sn_{0.9}In_{0.1}P₂O₇ particles in the matrix was relatively uniform, with no formation of pinholes observed. Fuel cell tests verified that the open-circuit voltage was maintained at a constant value of ~970 mV regardless of the electrolyte thickness (60–200 μm), while the Ohmic resistance was decreased to 0.24 Ω cm² by reducing the electrolyte thickness to 60 μm. The peak power densities achieved with unhumidified H₂ and air were 109 mW cm⁻² at 100 °C, 149 mW cm⁻² at 150 °C, and 187 mW cm⁻² at 200 °C. Furthermore, fuel cell performance was improved by hot-pressing an intermediate layer consisting of Sn_{0.9}In_{0.1}P₂O₇, Pt/C, TES-Oct, and (THS)Pro-SO₃H between the electrolyte and cathode.

© 2006 The Electrochemical Society. [DOI: 10.1149/1.2388737] All rights reserved.

Manuscript submitted June 28, 2006; revised manuscript received August 30, 2006. Available electronically November 17, 2006.

Fuel cells have received significant recent attention as next generation alternative energy sources because of their high energy conversion efficiencies and low emission of pollutants. Among the various types of fuel cells, polymer electrolyte fuel cells (PEFCs) can operate at low temperatures (<100 °C), allowing for rapid start-up. For this reason, PEFCs are considered to be the most suitable for fuel cells in vehicular and residential applications. However, many challenges still remain for realizing commercialization of PEFCs.¹ Because the most commonly used electrolyte in PEFCs, Nafion, is a hydrous proton conductor, it must be penetrated by large quantities of water molecules in the bulk to achieve high proton conductivities. Thus, it is necessary to operate the fuel cell under highly humidified conditions, requiring complicated water management in the fuel cell system. Furthermore, Pt anode catalysts are easily subjected to CO poisoning at such low temperatures, causing serious deterioration of the fuel cell. In addition, the necessity of using expensive Pt catalysts increases materials cost of the fuel cell. One approach to overcome these challenges is to develop anhydrous proton conductors capable of operating under dry conditions and at intermediate temperatures above 100 °C.² Considerable efforts are being currently expended towards the design of such proton conductors.^{3–8}

We have previously reported that an anhydrous proton conductor, 10 mol % In³⁺-doped SnP₂O₇ (Sn_{0.9}In_{0.1}P₂O₇), shows high proton conductivities above 10⁻¹ S cm⁻¹ between 100 and 300 °C under water-free conditions.^{9,10} This material was also explored for use as an electrolyte in some electrochemical devices. A fuel cell using the 0.35 mm thick Sn_{0.9}In_{0.1}P₂O₇ electrolyte membrane yielded a power density of 264 mW cm⁻² under unhumidified H₂/air conditions.¹¹ This material was also used as an electrolyte membrane in a deNO_x reactor¹² and a NO_x gas sensor.¹³ However, the electrolyte membranes used in these previous studies were merely prepared by pressing Sn_{0.9}In_{0.1}P₂O₇ powders into pellets, due to the difficulty in preparing sintered compacts of this material. The synthesis of a dense, flexible, and heat-resistant electrolyte membrane is a crucial requirement for practical applications of this material.

Forming hybrids of organic and inorganic materials is one of the promising methods that meet the above requirements, as they offer the possibility of improving mechanical and thermal properties of various difficult-to-consolidate inorganic materials.¹⁴ Indeed, several inorganic proton conductors have been investigated using composite

materials prepared by blending them with organic polymers.^{15–21} This approach also has an additional advantage of combining the positive features of each component via interactions at the molecular level. High proton transfer between clusters of the proton conductor in the matrix is expected if a material having acidic functions as proton sites is added as the third component.

In this study, we investigated the proton-conducting properties of organic/inorganic hybrid composite materials based on Sn_{0.9}In_{0.1}P₂O₇ in anhydrous environments. The starting materials chosen as the second and third components were 1,8-bis(triethoxysilyl)octane (TES-Oct) and 3-(triethoxysilyl)-1-propanesulfonic acid ((THS)Pro-SO₃H), respectively, which have previously been demonstrated to be excellent hybrid components.^{22,23} We also evaluated the performance of a fuel cell using the optimized composite material as an electrolyte membrane, wherein our interest is centered on fuel cell performance between 100 and 200 °C under unhumidified conditions.

Experimental

Synthesis of Sn_{0.9}In_{0.1}P₂O₇.— Sn_{0.9}In_{0.1}P₂O₇ was prepared as follows. SnO₂ and In₂O₃ powders were mixed with 85% H₃PO₄ and ion-exchanged water and held with stirring at 300 °C until the mixture formed a high viscosity paste. In this case, the H₃PO₄/MO_x (M = Sn and In) molar ratio was controlled to be 2.8, as a fraction of H₃PO₄ was lost by the subsequent heating treatment. The pastes were calcined in an alumina pot at 650 °C for 2.5 h and then ground with a mortar and pestle. The final P/(Sn + In) molar ratio of the compounds was confirmed to be 2.0 (±0.02) from X-ray fluorescence (XRF) measurements. For comparison with the composite membranes, the compound powders were pressed into pellets under a pressure of 2 × 10³ kg cm⁻², as shown in Fig. 1b.

Synthesis of hybrid composite membranes.— TES-Oct (Gelest. Inc., 0.14 g) was mixed with an equimolar amount of (THS)Pro-SO₃H (Gelest. Inc.) in 2-propanol according to procedures described in the literature.²³ Sn_{0.9}In_{0.1}P₂O₇ (1.15–2.19 g) and PTFE (0.06 g) was added to the solution and then kneaded in a mortar and pestle for further hydrolysis and condensation. The solution was cast onto a Teflon sheet and then cold-rolled to different thicknesses from 60 to 200 μm using a laboratory rolling mill. After peeling off the membrane, samples were cut with scissors with a size of 2 × 2 cm, as shown in Fig. 1a. A reference composite membrane free of (THS)Pro-SO₃H was also prepared using the same procedure as above.

* Electrochemical Society Student Member.

** Electrochemical Society Active Member.

^z E-mail: hibino@urban.env.nagoya-u.ac.jp

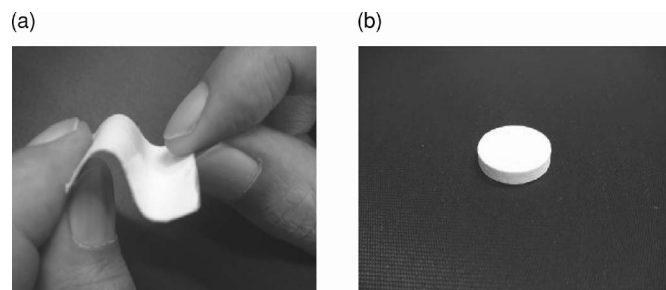


Figure 1. Photographs of (a) composite membrane ($\text{Sn}_{0.9}\text{In}_{0.1}\text{P}_2\text{O}_7$ content = 90 wt %) and (b) pellet samples.

Measurements.—The surface morphology of the membranes was determined using scanning electron microscopy (SEM) at a magnification of 10000x. The crystalline structure of the membranes was confirmed by X-ray diffraction (XRD). Impedance spectra measurements were carried out by the standard four probe method. The frequency range was 0.1 to 10^6 Hz, and the ac amplitude was 10 mV. Two types of galvanic cells, a H_2 concentration cell and a H_2 /air fuel cell, were fabricated using composite membranes with different thicknesses. Both the anode and cathode (area: 0.5 cm^2) consisted of a catalyst (10 wt % Pt/C, E-TEK) and carbon paper (Toray TGP-H-090), wherein the Pt loading was 0.6 mg cm^{-2} . The electromotive forces (EMFs) of the H_2 concentration cell were monitored as a function of temperature. The current-voltage curves of the fuel cell were measured by supplying unhumidified H_2 and air to the anode and cathode, respectively, at a flow rate of 30 mL min^{-1} . The Ohmic and polarization resistances were separated using a current interruption method. In this case, a Pt reference electrode was attached to one side of the electrolyte membrane, as illustrated in Fig. 2.

Results and Discussion

Figure 3 shows the Arrhenius plots of the conductivity of the composite membrane samples with various $\text{Sn}_{0.9}\text{In}_{0.1}\text{P}_2\text{O}_7$ contents in unhumidified air ($P_{\text{H}_2\text{O}} = \sim 0.0075 \text{ atm}$), including the data for a $\text{Sn}_{0.9}\text{In}_{0.1}\text{P}_2\text{O}_7$ pellet sample. The conductivity of the $\text{Sn}_{0.9}\text{In}_{0.1}\text{P}_2\text{O}_7$ -free composite membrane sample was $\sim 2 \times 10^{-4} \text{ S cm}^{-1}$ at all the tested temperatures, which is about two orders of magnitude lower than the value reported by Nishikawa et

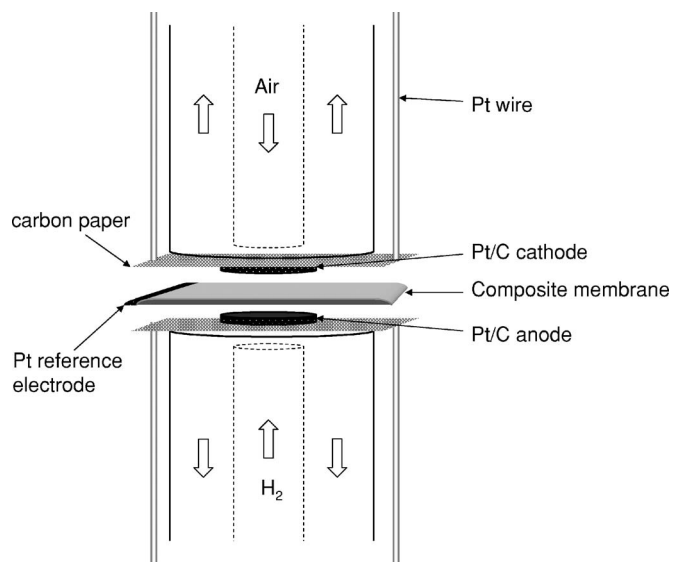


Figure 2. Schematic diagram showing the fuel cell testing assembly.

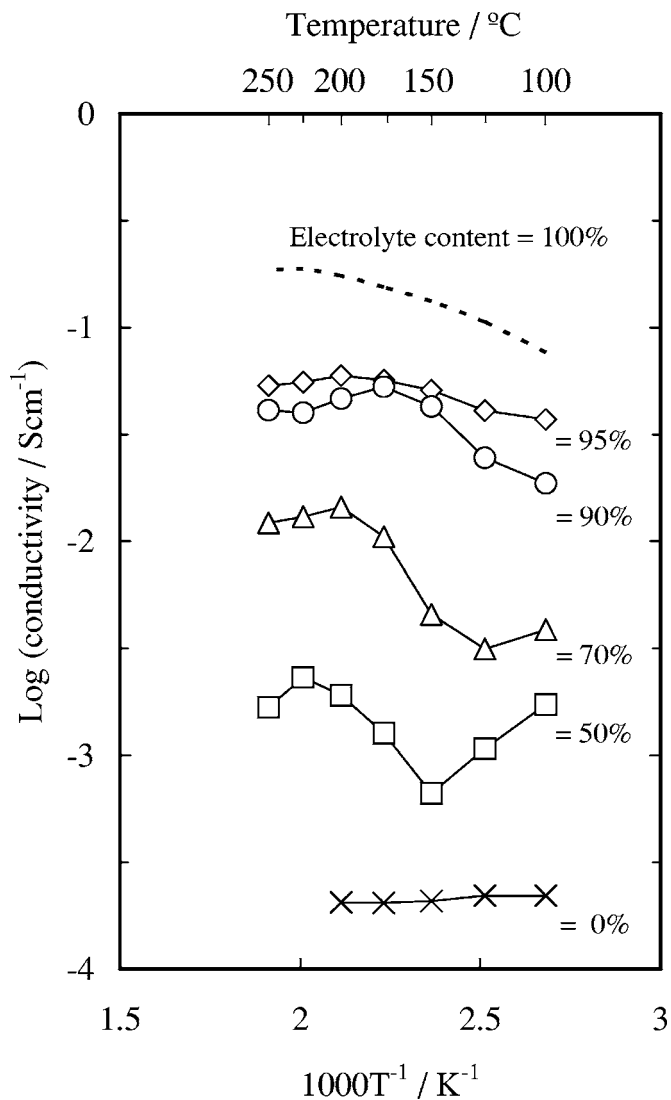


Figure 3. Arrhenius plots for conductivities of composite membrane samples having different $\text{Sn}_{0.9}\text{In}_{0.1}\text{P}_2\text{O}_7$ contents and the pellet sample. The samples were measured in unhumidified air.

al. at the same temperatures.²³ This can be explained by the differences in experimental conditions; Nishikawa et al. conducted their conductivity measurements at 100% relative humidity. The doping of $\text{Sn}_{0.9}\text{In}_{0.1}\text{P}_2\text{O}_7$ into the composite membrane significantly enhanced the conductivity, indicating that the doped $\text{Sn}_{0.9}\text{In}_{0.1}\text{P}_2\text{O}_7$ brought about proton conduction in the whole matrix. As a result, conductivities as high as 0.06 and 0.04 S cm^{-1} were obtained for $\text{Sn}_{0.9}\text{In}_{0.1}\text{P}_2\text{O}_7$ contents of 95 and 90 wt %, respectively, between 150 and 200°C . However, the flexibility of the composite membrane samples became low when the $\text{Sn}_{0.9}\text{In}_{0.1}\text{P}_2\text{O}_7$ content was 95 wt %. This may indicate that the organic polymer was no longer interconnected between the $\text{Sn}_{0.9}\text{In}_{0.1}\text{P}_2\text{O}_7$ clusters or particles, so that the hybrid effect appeared to disappear. To maintain both the conductivity and flexibility as high as possible, the optimum content of $\text{Sn}_{0.9}\text{In}_{0.1}\text{P}_2\text{O}_7$ was determined to be 90 wt %. Another significant result is that the composite membrane sample with 90 wt % $\text{Sn}_{0.9}\text{In}_{0.1}\text{P}_2\text{O}_7$ showed a lower conductivity of 0.02 S cm^{-1} in the absence of the (THS)Pro- SO_3H component, compared to the conductivity of 0.04 S cm^{-1} in the presence of the component. Given the structural similarity of the two composite membrane samples, the observed difference can be ascribed to the $-\text{SO}_3\text{H}$ groups avail-

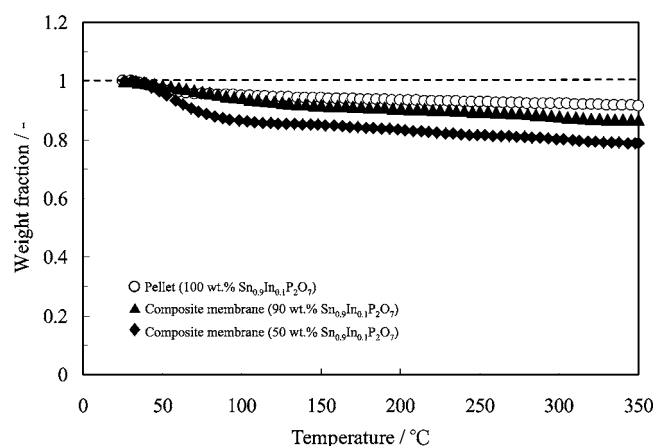


Figure 4. TG curves of $\text{Sn}_{0.9}\text{In}_{0.1}\text{P}_2\text{O}_7$ composite membrane and pellet samples.

able for proton transfer. The $-\text{SO}_3\text{H}$ group likely formed a proton-conducting pathway from one $\text{Sn}_{0.9}\text{In}_{0.1}\text{P}_2\text{O}_7$ cluster to another.

Figure 3 also shows that the composite membrane samples, especially with $\text{Sn}_{0.9}\text{In}_{0.1}\text{P}_2\text{O}_7$ contents of 50 and 70 wt %, revealed complex temperature dependence on the conductivity between 100 and 200°C, which was reproducible over temperature cycles. Moreover, the conductivities of all the composite membrane samples decreased with increasing temperature from 200 to 250°C, which was irreversible upon heating and cooling. We reasoned that while the former behavior is due to the dehydration of the membrane below 200°C, the later behavior is due to the thermal decomposition of components such as PTFE above 200°C. Evidence for this reasoning is provided by the thermogravimetry (TG) analysis of the composite membrane and pellet samples. As can be seen from Fig. 4, the composite membrane sample with 50 wt % $\text{Sn}_{0.9}\text{In}_{0.1}\text{P}_2\text{O}_7$ showed a large decrease in the weight fraction below 100°C resulting from the desorption of water. In addition, the weight fractions of both the composite membrane samples were slightly more decreased above 250°C than that of the pellet sample, indicating the weight loss of components except for $\text{Sn}_{0.9}\text{In}_{0.1}\text{P}_2\text{O}_7$. From the above results, the composite membrane sample with 90 wt % $\text{Sn}_{0.9}\text{In}_{0.1}\text{P}_2\text{O}_7$ was used below 200°C in subsequent experiments.

Structural and morphological characterization of the $\text{Sn}_{0.9}\text{In}_{0.1}\text{P}_2\text{O}_7$ composite membrane and pellet samples was carried out using XRD and SEM, respectively. Figures 5a and b show XRD profiles of the composite membrane and pellet samples, respectively.

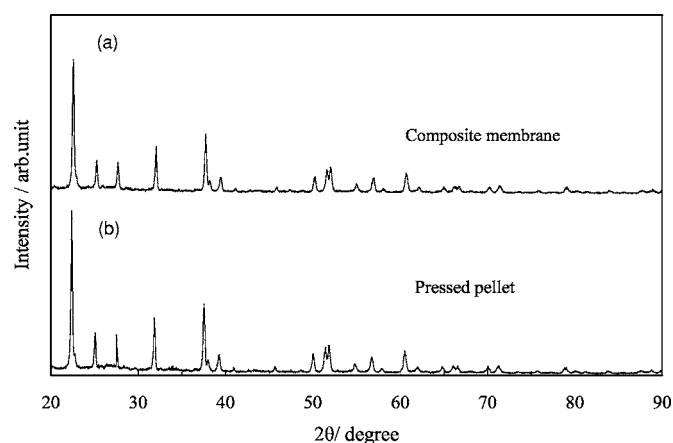


Figure 5. XRD patterns of (a) $\text{Sn}_{0.9}\text{In}_{0.1}\text{P}_2\text{O}_7$ composite membrane and (b) pellet samples.

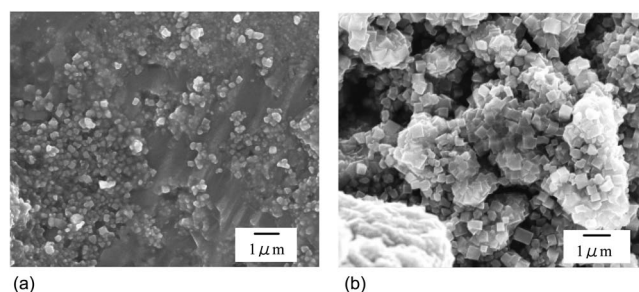


Figure 6. SEMs of (a) $\text{Sn}_{0.9}\text{In}_{0.1}\text{P}_2\text{O}_7$ composite membrane and (b) pellet samples.

The pellet sample showed the same patterns as those for SnP_2O_7 reported in the literature.²⁴ Also, a slight shift toward lower angles was observed in the peaks for our sample with respect to SnP_2O_7 , indicating an increasing lattice constant due to the doping of In^{3+} in place of Sn^{4+} . On the other hand, the peaks observed for the composite membrane sample were almost identical to those of the pellet sample. This suggests that the polymer components exist as an amorphous phase in the matrix. Figures 6a and b show SEMs of the composite membrane and pellet sample, respectively. The surface of the pellet sample was highly porous, which corresponds to the relative density value of 79.3% determined by dividing the bulk density of the sample by the theoretical density. However, the composite membrane was rather compact, as observed in Fig. 6a, suggesting that the polymer functioned as a binder at the interface. Although the distribution of $\text{Sn}_{0.9}\text{In}_{0.1}\text{P}_2\text{O}_7$ in the matrix is difficult to visualize by surface SEM, homogeneity ranging from several micrometers to several decades of micrometers was likely established, as will be described later.

The galvanic cell method was used for the electrochemical characterization of the $\text{Sn}_{0.9}\text{In}_{0.1}\text{P}_2\text{O}_7$ composite membrane and pellet samples. The following galvanic cell was fabricated using each sample as an electrolyte



Here, we used relatively thick electrolyte samples in order to reduce the influence of gas leakage through the electrolyte—200 μm for the composite membrane and 2.1 mm for the pellet. A comparison of the measured EMF values with the theoretical values calculated from Nernst's equation between 100 and 200°C is shown in Fig. 7. It was found that all the EMF values obtained for both

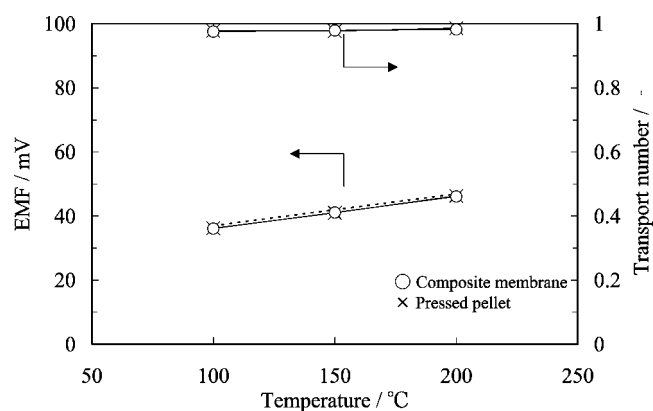


Figure 7. EMFs of H_2 concentration cells with $\text{Sn}_{0.9}\text{In}_{0.1}\text{P}_2\text{O}_7$ composite membrane and pellet samples, and their proton transport number as a function of temperature. Both the H_2 and H_2 -Ar mixture used were unhumidified.

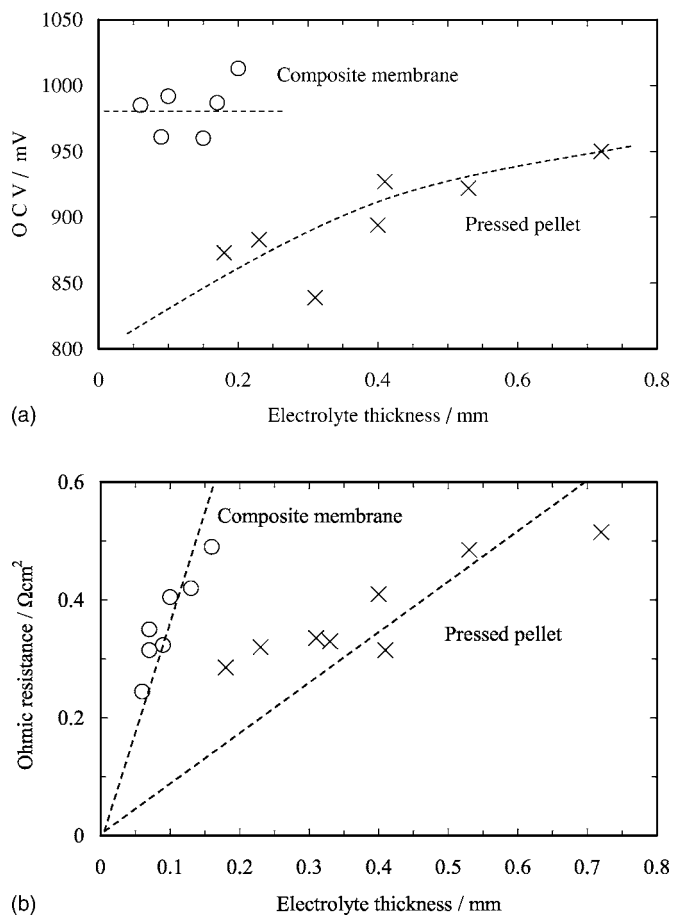


Figure 8. (a) OCVs and (b) Ohmic resistance of fuel cells with $\text{Sn}_{0.9}\text{In}_{0.1}\text{P}_2\text{O}_7$ composite membrane and pellet samples at 200°C as a function of electrolyte thickness. Both H_2 and air were unhumidified.

samples were very close to the corresponding theoretical values. We estimated the proton transport number from the ratio of the EMF value to the theoretical value as

$$t_{\text{H}^+} = \text{EMF}_{\text{observed}} / \text{EMF}_{\text{theoretical}} \quad [2]$$

This method is valid, especially when the ion transport number is high because the observed EMF value is determined mainly by the Ohmic resistance of the charge carrier. The estimated proton transport numbers of the two samples were in the range of 0.96–0.98 for both the samples, indicating that the composite membrane as well as pellet are substantially pure proton conductors in H_2 atmospheres. In other words, the polymer does not retard the proton transport number of $\text{Sn}_{0.9}\text{In}_{0.1}\text{P}_2\text{O}_7$ at all.

Another galvanic cell was fabricated using the $\text{Sn}_{0.9}\text{In}_{0.1}\text{P}_2\text{O}_7$ composite membrane and pellet samples with varying thickness values

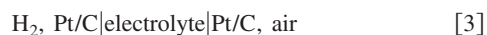


Figure 8a shows the influence of the electrolyte thickness on the open-circuit voltage (OCV) obtained for the two fuel cells at 200°C. A decrease in the OCV with decreasing electrolyte thickness was observed for the pellet sample, implying that H_2 or O_2 crossover through the electrolyte increases with decreasing electrolyte thickness. In contrast, the OCVs for the composite membrane were almost independent of the electrolyte thickness. This result indicates that both H_2 and O_2 crossovers through the electrolyte are negligible, which is consistent with the SEM shown in Fig. 6. However, the OCVs for the composite membranes were ~ 970 mV, which is lower than the theoretical value of 1.1 V. As reported previously,⁹

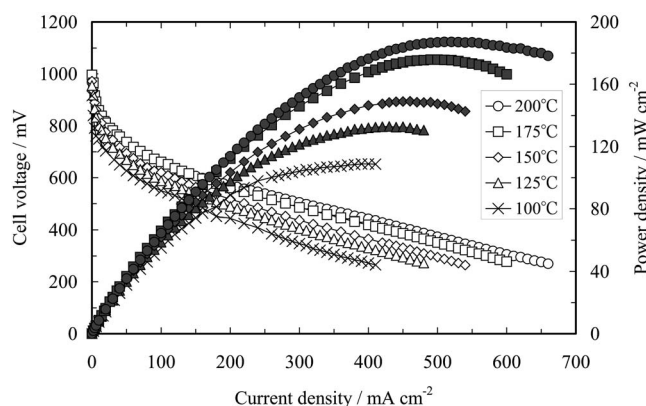


Figure 9. Cell voltage and power density vs current density of fuel cells with the composite membrane between 100 and 200°C. Unhumidified H_2 and air were supplied to the anode and cathode, respectively, at a flow rate of 30 mL min^{-1} . The electrolyte thickness was $60 \mu\text{m}$.

while the conductivity of $\text{Sn}_{0.9}\text{In}_{0.1}\text{P}_2\text{O}_7$ was almost independent of P_{O_2} from 10^{-22} to 10^{-3} atm, it increased gradually with increasing P_{O_2} from 10^{-3} to 1 atm. Consequently, the observed lower OCV values can be considered to be due to partial electron-hole conduction in the electrolyte, causing an internal short circuit of the fuel cell.²⁵

Figure 8b shows the influence of the electrolyte thickness on the Ohmic resistance obtained for the two fuel cells at 200°C. The Ohmic resistances of the two samples roughly linearly decreased with decreasing electrolyte thickness. In particular, the composite membrane showed linearity over the thickness range from 60 to $150 \mu\text{m}$, assuming that the $\text{Sn}_{0.9}\text{In}_{0.1}\text{P}_2\text{O}_7$ powders were homogeneously distributed at the $\sim 10 \mu\text{m}$ level in the matrixes. The Ohmic resistance values of the composite membrane samples were always higher than those of the pellet samples at the same electrolyte thickness, reflecting the difference in the proton conductivity for the two samples. However, we emphasize that the composite membrane sample showed a relatively low resistance of $0.24 \Omega \text{ cm}^2$, while maintaining a high OCV of 986 mV, which could not be achieved for the pellet sample.

An additional objective of this study was to investigate the fuel cell performance at intermediate temperatures. Fuel cell tests were conducted using the $60 \mu\text{m}$ thick $\text{Sn}_{0.9}\text{In}_{0.1}\text{P}_2\text{O}_7$ composite membrane as an electrolyte between 100 and 200°C under unhumidified conditions. The current-voltage curves of the fuel cell are shown in Fig. 9. At all of the tested temperatures, OCVs above 950 mV were obtained, and no limiting current behavior was observed at high current densities. In addition, the current-voltage slopes became lower as the operating temperature increased. The peak power density thus reached 109 mW cm^{-2} at 100°C, 149 mW cm^{-2} at 150°C, and 187 mW cm^{-2} at 200°C. However, the power densities were much lower compared to those expected from the Ohmic resistances (as an example, $0.24 \Omega \text{ cm}^2$ at 200°C) of the electrolyte, which may be ascribed to the large polarization resistance of the fuel cell.

To understand the above results, we measured the anodic and cathodic overpotentials by the current interruption method. It can be seen from Fig. 10 that the overpotentials were always dominated by the cathode in the temperature range of 100–200°C; the cathodic overpotentials were estimated to account for 83–85% of the overall voltage drops during the cell discharge. On the other hand, the anodic overpotentials (as well as the IR drops, although the data is not shown in Fig. 10) negligibly affected the voltage drops especially at higher temperatures. Clearly, the development of a more active cathode is required to improve the fuel cell performance. Note that water formed electrochemically did not affect the subsequent cathode reaction because the discharge at high current densities gave rise to no limiting currents. It is likely that the charge-transfer reaction of oxy-

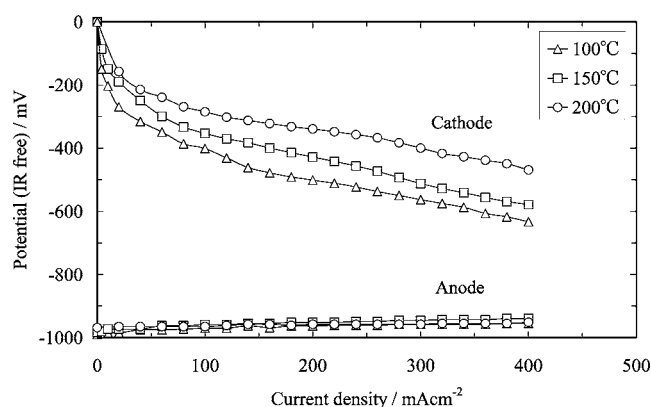


Figure 10. Anodic and cathodic overpotentials vs current density of fuel cells with the composite membrane between 100 and 200°C. The experimental conditions were the same as in Fig. 9.

gen reduction at the electrolyte/electrode interface proceeded at a very slow rate. Also, note that only the cathode was in physical contact with the electrolyte, probably resulting in low-density three phase boundaries (TPBs). Thus, it is necessary to optimize the electrolyte/electrode interface.

We have previously reported that the cathodic overpotential could be reduced by applying an intermediate layer consisting of $\text{Sn}_{0.9}\text{In}_{0.1}\text{P}_2\text{O}_7$ and Pt/C powders at the electrolyte/electrode interface in the $\text{Sn}_{0.9}\text{In}_{0.1}\text{P}_2\text{O}_7$ pellet-based fuel cell.¹¹ An attempt was made to hot-press the intermediate layers constructed from $\text{Sn}_{0.9}\text{In}_{0.1}\text{P}_2\text{O}_7$, Pt/C, TES-Oct, and (THS)Pro- SO_3H between the electrolyte and cathode. As a result of the optimization of the weight ratio of the $\text{Sn}_{0.9}\text{In}_{0.1}\text{P}_2\text{O}_7$ electrolyte to the Pt/C catalyst, the cathodic overpotential was shown to be the most improved when $\text{Sn}_{0.9}\text{In}_{0.1}\text{P}_2\text{O}_7$:Pt/C = 20:1. A comparison of the presence or absence of the intermediate layer at 150°C is shown in Fig. 11. The voltage drop was reduced by using the intermediate layer, so that the peak power density increased from 149 to 197 mW cm^{-2} . Similar effects were obtained at other temperatures, although these were smaller at higher temperatures. One can consider that such performance gains are due to an increase in the area of the three-phase

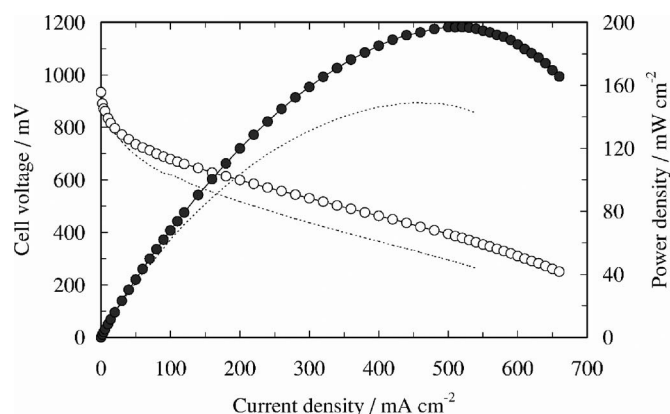


Figure 11. Cell voltage and power density vs current density of improved fuel cells with the composite membrane at 150°C. The dotted lines show the results for the fuel cell without any intermediate layer. The experimental conditions were the same as in Fig. 9.

boundary for the cathode reaction. Indeed, the total polarization resistance decreased by 1.3 $\Omega \text{ cm}^2$ at 150°C by applying the intermediate layer. One may also expect that the fuel cell performance is further enhanced by improving the microstructure, catalytic activity, and proton conductivity of the intermediate layer.

Conclusions

Organic/inorganic hybrid composite membranes based on $\text{Sn}_{0.9}\text{In}_{0.1}\text{P}_2\text{O}_7$ were investigated for intermediate-temperature fuel cells. 1,8-bis(triethoxysilyl)octane and 3-(triethoxysilyl)-1-propanesulfonic acid were chosen as polymer precursors. The composite membrane prepared at a $\text{Sn}_{0.9}\text{In}_{0.1}\text{P}_2\text{O}_7$ content of 90 wt % showed a proton conductivity of 0.04 S cm^{-1} at 175°C in an unhumidified atmosphere. The membrane was also found to be flexible. $\text{Sn}_{0.9}\text{In}_{0.1}\text{P}_2\text{O}_7$ powders were relatively homogeneously packed in the matrix, with no pores visible. The proton transport numbers of the composite membrane estimated by the EMF technique were 0.96–0.98 between 100 and 200°C. A fuel cell with the composite membrane maintained the OCV at an almost constant value of 970 mV regardless of the electrolyte thickness and also showed a decreasing Ohmic resistance with decreasing electrolyte thickness. The resulting peak power density reached 109 mW cm^{-2} at 100°C, 149 mW cm^{-2} at 150°C, and 187 mW cm^{-2} at 200°C. Furthermore, a membrane electrode assembly fabrication technique offered the potential for enhancing the fuel cell performance.

Nagoya University assisted in meeting the publication costs of this article.

References

- B. C. H. Steele and A. Heinzel, *Nature (London)*, **414**, 345 (2001).
- J. S. Wainright, M. H. Litt, and R. F. Savinell, in *Handbook of Fuel Cells—Fundamentals, Technology, Applications*, W. Vielstich, A. Lamm, and H. Gasteiger, Editors, Wiley (2003).
- T. Kenjo and Y. Ogawa, *Solid State Ionics*, **76**, 29 (1995).
- S. M. Haile, D. A. Boysen, C. R. I. Chisholm, and R. B. Merle, *Nature (London)*, **410**, 910 (2001).
- T. Matsui, S. Takeshita, Y. Iriyama, T. Abe, M. Inaba, and Z. Ogumi, *Electrochem. Commun.*, **6**, 180 (2004).
- D. A. Boysen, T. Uda, C. R. I. Chisholm, and S. M. Haile, *Science*, **303**, 68 (2004).
- W. Wiczcerek, G. Zukowska, R. Borkowska, S. H. Chung, and S. Greenbaum, *Electrochim. Acta*, **46**, 1427 (2001).
- A. Matsuda, T. Kanzaki, K. Tadanaga, M. Tatsumisago, and T. Minami, *Solid State Ionics*, **154–155**, 687 (2002).
- M. Nagao, A. Takeuchi, P. Heo, T. Hibino, M. Sano, and A. Tomita, *Electrochem. Solid-State Lett.*, **9**, A105 (2006).
- M. Nagao, T. Kamiya, P. Heo, A. Tomita, T. Hibino, and M. Sano, *J. Electrochem. Soc.*, **153**, A1604 (2006).
- P. Heo, H. Shibata, M. Nagao, T. Hibino, and M. Sano, *J. Electrochem. Soc.*, **153**, A897 (2006).
- M. Nagao, T. Yoshii, T. Hibino, M. Sano, and A. Tomita, *Electrochem. Solid-State Lett.*, **9**, J1 (2006).
- M. Nagao, Y. Namekata, T. Hibino, M. Sano, and A. Tomita, *Electrochem. Solid-State Lett.*, **9**, H48 (2006).
- A. Okada and A. Usuki, *Mater. Sci. Eng., C*, **3**, 109 (1995).
- P. Staiti, M. Minutoli, and S. Hocevar, *J. Power Sources*, **90**, 231 (2000).
- G. Alberti, M. Casciola, and R. Palombari, *J. Membr. Sci.*, **172**, 233 (2000).
- B. Bonnet, D. J. Jones, J. Rozière, L. Tchicaya, G. Alberti, M. Casciola, L. Massinelli, B. Bauer, A. Ieraio, and E. Ramunni, *J. New Mater. Electrochem. Syst.*, **3**, 87 (2000).
- J. D. Kim and I. Honma, *Electrochim. Acta*, **48**, 3633 (2003).
- D. R. Vernon, F. Meng, S. F. Dec, D. L. Williamson, J. A. Turner, and A. M. Herring, *J. Power Sources*, **139**, 141 (2005).
- M. Nagai and Y. Chiba, *Solid State Ionics*, **76**, 2991 (2005).
- J. D. Kim, T. Mori, and I. Honma, *J. Electrochem. Soc.*, **153**, A508 (2006).
- H. Nakajima, S. Nomura, T. Sugimoto, S. Nishikawa, and I. Honma, *J. Electrochem. Soc.*, **149**, A953 (2002).
- O. Nishikawa, T. Sugimoto, S. Nomura, K. Doyama, K. Miyatake, H. Uchida, and M. Watanabe, *Electrochim. Acta*, **50**, 667 (2004).
- P. K. Gover, N. D. Withers, S. Allen, R. L. Withers, and S. O. Evans, *J. Solid State Chem.*, **166**, 42 (2002).
- S. Hamakawa, T. Hibino, and H. Iwahara, *J. Electrochem. Soc.*, **141**, 1720 (1994).